UAB
Universitat Autònoma de Barcelona

Dipòsit digital de documents de la UAB

This is the **accepted version** of the journal article:

Chang, Xingqi; Chacón-Borrero, Jesús; Shang, Jian; [et al.]. «Improved Mn4+/Mn2+ Contribution in High-Voltage Zn-MnO2 Batteries Enabled by an Al3+-Ion Electrolyte». Advanced Energy Materials, Vol. 14, Issue 48 (December 2024), art. 2402584. DOI 10.1002/aenm.202402584

This version is available at https://ddd.uab.cat/record/310024

under the terms of the IN COPYRIGHT license

Improved Mn^{4+}/Mn^{2+} contribution in high-voltage Zn-MnO_2 batteries enabled by an Al^{3+}-ion electrolyte

Xingqi Chang [a,b,†], Jesús Chacón-Borrero [a,†], Ke Xiao [a], Guillem Montaña-Mora [a], Karol V. Mejia-Centeno [a,b], Xuan Lu [a], Ao Yu [a], Jing yu [a,c], Xiaolong Zhou [d,], Sarayut Tunmee [e], Pinit Kidkhunthod [e], Changcai Cui [f], Junshan Li [g], Yongbing Tang [d,*], Paulina R. Martínez-Alanis [a], Jordi Arbiol [c,h] and Andreu Cabot [a,h,*]*

[a] Catalonia Institute for Energy Research – IREC, Sant Adrià de Besòs, Barcelona 08930, Spain.

[b] Facultat de Química, Universitat de Barcelona, Carrer de Martí i Franquès, Barcelona 08028, Spain.

[c] Catalan Institute of Nanoscience and Nanotechnology (ICN2), CSIC and BIST, Campus UAB, Bellaterra 08193, Barcelona, Spain.

[d] Advanced Energy Storage Technology Research Center, Shenzhen Institute of Advanced Technology, Chinese Academy of Sciences, Shenzhen, 518055, China.

[e] Synchrotron Light Research Institute (Public Organization), 111 University Avenue, Muang District, Nakhon Ratchasima 30000, Thailand.

[f] Institute of Manufacturing Engineering, Huaqiao University, Xiamen, China.

[g] Institute for Advanced Study, Chengdu University, 610106, Chengdu, China.

[h] ICREA Pg. Lluis Companys, 08010 Barcelona, Catalonia, Spain.

[†] X.Q. Chang and J. A. Chacón contributed equally to this work.

[*] Correspondence: zhouxl@siat.ac.cn, tangyb@siat.ac.cn; acabot@irec.cat.

Keywords: Al-ion, Mn^{4+}/Mn^{2+} reaction, hybrid ions, Zn-MnO_2 battery, Zn-ion battery, MnO_2

Abstract

Rechargeable aqueous Zn-MnO_2 batteries are gaining widespread interest as a cost-effective and safe energy storage solution. However, their commercialization is hindered by the limited stability, output voltage and energy densities experimentally obtained. Herein, we propose a hybrid ion Zn-MnO_2 system with enhanced Mn^{4+}/Mn^{2+} electrochemical contribution enabled by an Al^{3+}-based electrolyte. Compared with previous Zn-MnO_2 batteries based on Zn^{2+} electrolytes, the hybrid Al^{3+}/Zn^{2+} ion cell is characterized by a higher output voltage of 1.75 V, capacities up to 469 $mAh \cdot g^{-1}$, and outstanding energy densities up to ~730 $Wh \cdot kg^{-1}$ at 0.3 $A \cdot g^{-}$

[1] (mass based on cathode material). Besides, the Al^{3+}-enabled Zn-MnO_2 battery shows 100% capacity and energy density retention after 10,000 cycles at 2 $A \cdot g^{-1}$. Even at a high mass–loading of 6.2 $mg \cdot cm^{-2}$, a capacity of ~200 $mAh \cdot g^{-1}$ is maintained for over 100 cycles. This outstanding performance is related to the contribution of different intercalation and reaction mechanisms, as proved by the combination of electrochemical analysis and *ex situ* x-ray diffraction characterization of the cells at different discharge stages. Al^{3+} ions, as Lewis strong acid, contribute to capacity in two significant ways: through a highly reversible intercalation/de-intercalation that substantially boosts capacitance at low current rates, and promoting the Mn^{4+}/Mn^{2+} reaction aided by H^+ that dominates the capacitance at higher current rates. Overall, this work demonstrates a practical Zn-MnO_2 battery with a high potential for low-cost stationary energy storage habilitated by multiple ion co-intercalation.

1. Introduction

The utilization of alternative monovalent (Na^+, K^+) or multivalent (Zn^{2+}, Mg^{2+}, Ca^{2+}, Al^{3+}) cations in energy storage devices has garnered significant interest owing to the drawbacks associated with lithium, such as its limited availability and related high-cost.[1] Rechargeable batteries based on multivalent metal–ions are particularly attractive because of their abundance in the Earth's crust and the associated multi-electron transfer processes. On the other hand, from cost, environmental impact and safety perspectives, aqueous systems are especially appealing. In this scenario, the development of aqueous zinc-based rechargeable batteries is gaining momentum driven by the inherently high theoretical capacity of zinc metal anodes (5851 $mAh \cdot mL^{-1}$ in volume and 820 $mAh \cdot g^{-1}$ in mass), the small ionic radius of Zn^{2+} (0.74 Å), and the abundance, low cost, simple processing, and safety of Zn.[2] In addition, Zn shows excellent compatibility with aqueous electrolytes, with a convenient redox potential (–0.763 V vs. standard hydrogen electrode) and excellent Zn/Zn^{2+} redox reversibility related to the inhibition of the hydrogen evolution reaction (HER) on its surface.[3] Considering all these advantages, aqueous zinc–ion batteries are particularly appealing in large-scale storage systems, among other applications.[4]

At the cathode side of aqueous Zn-based batteries, the use of manganese oxides offers advantages in terms of average voltage (~1.3 V vs. Zn^{2+}/Zn), theoretical capacity (~308 $mAh \cdot g^{-1}$, $Zn_{0.5}MnO_2$), cost, discharge potential, and cycle/rate performance.[5] However, the specific energy of current Zn-MnO_2 batteries remains unsatisfactory at approximately 70-140 $Wh \cdot kg^{-1}$, whereas the values obtained from commercial Li-ion batteries are around 180-230 $Wh \cdot kg^{-1}$.[6]

The moderate average discharge potential (ADV) of current MnO_2 cathodes vs. the Zn anode, at about 1.3~1.4 V vs. $Zn^{2+/}Zn$,[7-10] is a main factor currently limiting the energy density of Zn-MnO_2 batteries [11].

Zinc sulfate ($ZnSO_4$), chloride ($ZnCl_2$), perchlorate ($ZnClO_4$), and trifluoromethanesulfonate ($Zn(OTf)_2$) are the commonly used electrolytes in aqueous zinc-ion batteries. Among them, while $ZnCl_2$ and $ZnClO_4$ are strongly acidic and corrosive, the alkaline nature of $Zn(OTf)_2$ makes it more gentle with the anode but favors the growth of irreversibly discharged $Mn(OH)_2$ at the cathode. On the other hand, $ZnSO_4$ aqueous electrolytes have a weak acidic character that enables H^+ intercalation to contribute to the capacity. Besides, during the discharge, $Zn_4SO_4(OH)_6{\cdot}5H_2O$ precipitates, protecting the cathode surface and buffering the electrolyte pH.[12]

Within Zn-MnO_2 batteries, additional capacity contribution can be obtained through Mn^{2+} deposition and dissolution.[13] Thus, to further enhance the energy density and electrochemical stability of Zn-MnO_2 batteries, Mn^{2+} ions can be introduced as electrolyte additive.[14] The addition of an extra ion participating in the charge/discharge process substantially improves the rate and cycling performance of Zn-MnO_2 batteries. Mn^{2+} ions transform to MnOOH (~1.3 V vs. Zn^{2+}/Zn) during the discharge process and MnOOH transforms to MnO_2 (~1.8 V vs. Zn^{2+}/Zn) during the charge process.[15] Thus Mn^{2+} ions enable MnOOH to reversibly transform into MnO_2 but with no discharge capacity contribution in the high voltage range. Thus, while Zn-MnO_2 batteries have room for increasing the discharge voltage plateau in weakly acidic aqueous electrolytes, to overcome the current limitations of Zn-MnO_2 batteries, new approaches should be developed.

Herein, we describe a novel hybrid ion Zn-MnO_2 battery that employs an Al^{3+}-based electrolyte. Compared with conventional Zn-MnO_2 batteries, the Al^{3+}/Zn^{2+} hybrid device proposed here enables larger capacities, a higher discharge voltage plateau, improved energy densities, and extended stability. In this direction, we test different aluminum salts and concentrations to find the optimum electrolyte. Besides, the outstanding performance obtained is rationalized using *ex situ* X-ray diffraction (XRD) analyses of the cells at different discharge stages, demonstrating reversible participation of Al^{3+} in battery cycling that enables a highly reversible Mn^{4+}/Mn^{2+} reaction in the MnO_2 electrode.

2. Results and Discussion

Composites of multi-walled carbon nanotubes (CNTs) and elongated and flat MnO_2 particles (MnO_2/CNT) were produced via a facile hydrothermal method (see details in the Experimental Section in the supporting information, SI). HRTEM (Figure 1a,b) and XRD (Figure 1c) characterization of the composites show the presence of the layered birnessite-MnO_2 phase (δ-MnO_2, JCPDS card Nº 043-1456). The high-resolution Mn 2p XPS spectrum of δ-MnO_2/CNT displays a doublet centered at 654.2 eV and 642.5 eV that can be assigned to a Mn^{4+} chemical state (Figure S1).[16] The Mn K-edge X-ray absorption near edge structure (XANES) spectra of δ-MnO_2/CNT and three reference manganese oxides are shown in Figure 1d. The peak located at 6560.7 eV of δ-MnO_2/CNT overlaps with that of the MnO_2 standard material, confirming the Mn^{4+} chemical state.[17,18]

The suitability of different Al^{3+} aqueous electrolytes was initially tested using linear sweep voltammetry (LSV) at a scan rate of 5 $mV \cdot s^{-1}$ in a three-electrode configuration to investigate the HER on the Zn foil used as the working electrode. A platinum mesh was used as the counter electrode and Ag/AgCl (saturated KCl) as the reference electrode. Different Al^{3+} aqueous electrolytes were tested: 1M aluminum sulfate electrolyte (ASE), 2M aluminum trifluoromethanesulfonate electrolyte (ATE), and 2M aluminum perchlorate electrolyte (APE). As shown in Figure 2a, the three Al-based electrolytes tested were much more acidic (pH values of 2.2, 1.1, and 1.1 for ASE, ATE, and APE, respectively) than the standard 2M zinc sulfate electrolyte (ZSE) conventionally used in aqueous Zn-ion batteries (pH = 4.7). Additional 2M $AlCl_3$ and 2M $Al(Ac)_3$ aqueous electrolytes were also initially considered, but they provided negligible capacity and thus were discarded (Figure S2). LSV curves (Fig. 2b and 2c) show ASE to provide the best performance in terms of the highest HER overpotential (η, –976 mV) compared with APE (–822 mV) and ATE (–902 mV).[19-21] This is consistent with the $ZnSO_4$ also providing the best performance among the different Zn^{2+} salts, associated with the high electrochemical stability of SO_4^{2-} ions and their ability to adsorb at anode and cathode surfaces forming a protective layer that avoids the corrosion of the Zn anode surface. [22,23]

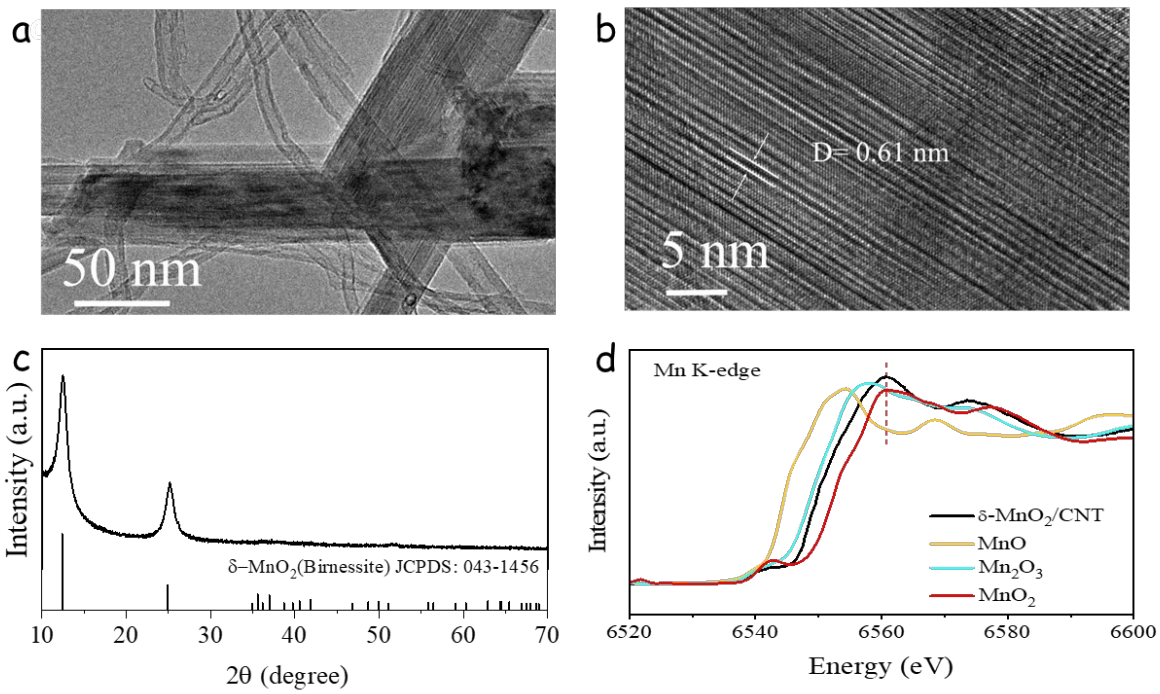

Figure 1. (a) TEM and (b) HRTEM images of the δ-MnO_2/CNT composite. The lattice fringes in the HRTEM image show an interlayer distance of ~0.61 nm, which fits the (001) interplane distance of δ–MnO_2. (c) XRD peaks of δ-MnO_2/CNT (d) Mn K-edge XANES spectrum of δ-MnO_2/CNT and MnO_2, Mn_2O_3, and MnO standard samples.

The electrochemical performance of the Zn-MnO_2 systems with different Al-ion electrolytes was tested using coin cells assembled using a MnO_2/CNT cathode, a Zn foil anode, and the different Al^{3+} aqueous electrolytes (see details in SI). Their electrochemical performance was evaluated by galvanostatic charge/discharge cycles and cyclic voltammetry (CV). As observed in Figure 2d, in the first galvanostatic charge-discharge process, the coin cells with different Al-based electrolytes show one sloping discharge plateau at ~1.65 V for ASE, ~1.36 V for ATE, and ~1.51 V for APE. Their open circuit voltage (OCV) was 1.74 V for ASE, 1.63 V for ATE, and 1.58 V for APE.

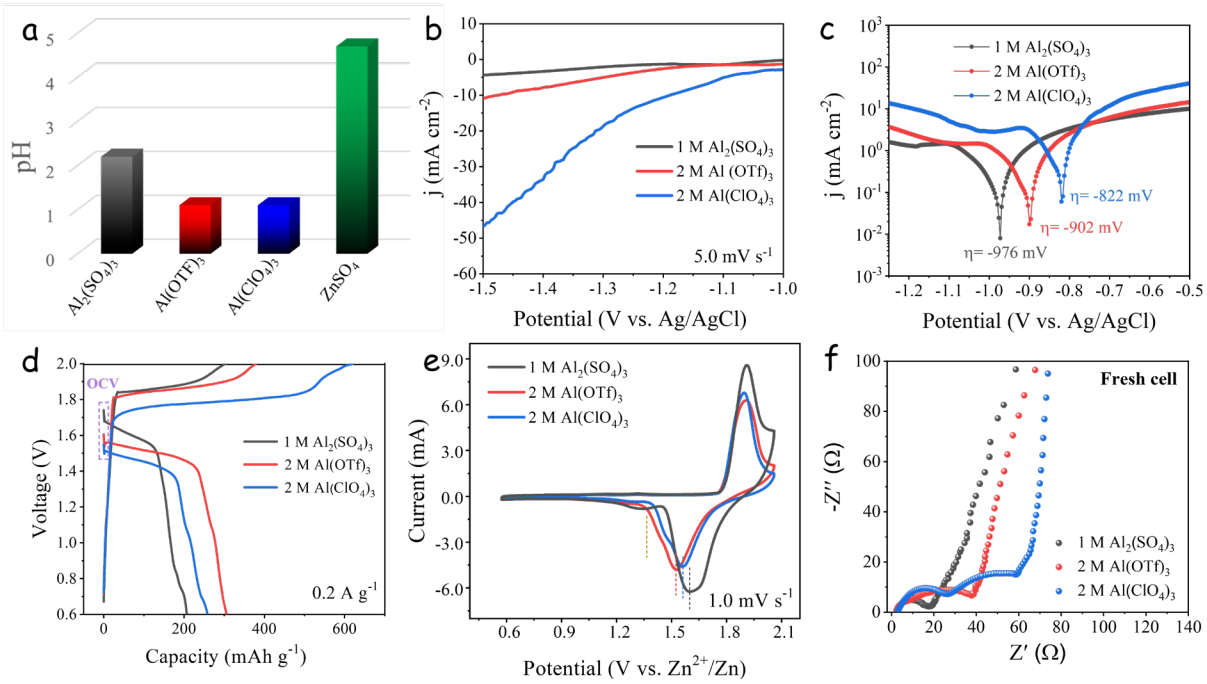

Figure 2. Comparison of the performance of Zn-MnO_2 batteries with different Al-based electrolytes: (a) Electrolyte pH values, (b) LSV curves at 5 mV·s^{-1}. (c) Tafel curves. (d) First galvanostatic discharge-charge curves, (e) First CV curves at 1 mV·s^{-1} with 0.6–2.1 V of voltage window. (f) EIS curves of fresh cells.

From an electrochemical point of view, when no current flows and the electrode potentials are in an equilibrium state, the OCV of a full cell can be determined as:

$$OCV = V_{anode}^{eq} - V_{cathode}^{eq} \quad (1)$$

CV curves at 1.0 mV s^{-1} (Figure 2e) show the cells with the Al-ion electrolytes to display one cathodic and one anodic peak in the voltage range tested (0.6 V - 2.1 V). While the anodic peak remained invariable at 1.9 V for the different electrolytes, the cathodic peak was obtained at around ~1.60 V, ~1.56 V, and ~1.52 V for ASE, ATE, and APE, respectively. Besides, the EIS spectra obtained from the fresh cells (Figure 2f) show that the ASE provides the lowest impedance related to a higher reversibility.

As shown in Figure 3a, the ASE also enabled Zn-MnO_2 cells with higher cycling stability at 1.0 A·g^{-1}. After undergoing 500 cycles, the capacity of the ASE-based cell exceeds its initial capacity. In contrast, the capacity of ATE- and APE-based cells decayed quickly. The rate performance of the ASE-based coin cells is displayed in Figures 3b and 3c. ASE-based cells show excellent rate capability, with discharge capacities of 234, 192, 164, 147, 132, and 116 mAh·g^{-1} at 0.4, 0.8, 1.2, 1.5, 2.0 and 3 A·g^{-1}, respectively. Besides, the discharge plateau is

maintained above 1.5 V in the current range of 0.4 to 3.0 $A \cdot g^{-1}$. Benefiting from the high discharge plateau and specific capacity, outstanding energy densities of ~384 $Wh \cdot kg^{-1}$ at 0.4 $A \cdot g^{-1}$ and ~165 $Wh \cdot kg^{-1}$ at 3.0 $A \cdot g^{-1}$, based on the cathode mass, were determined.

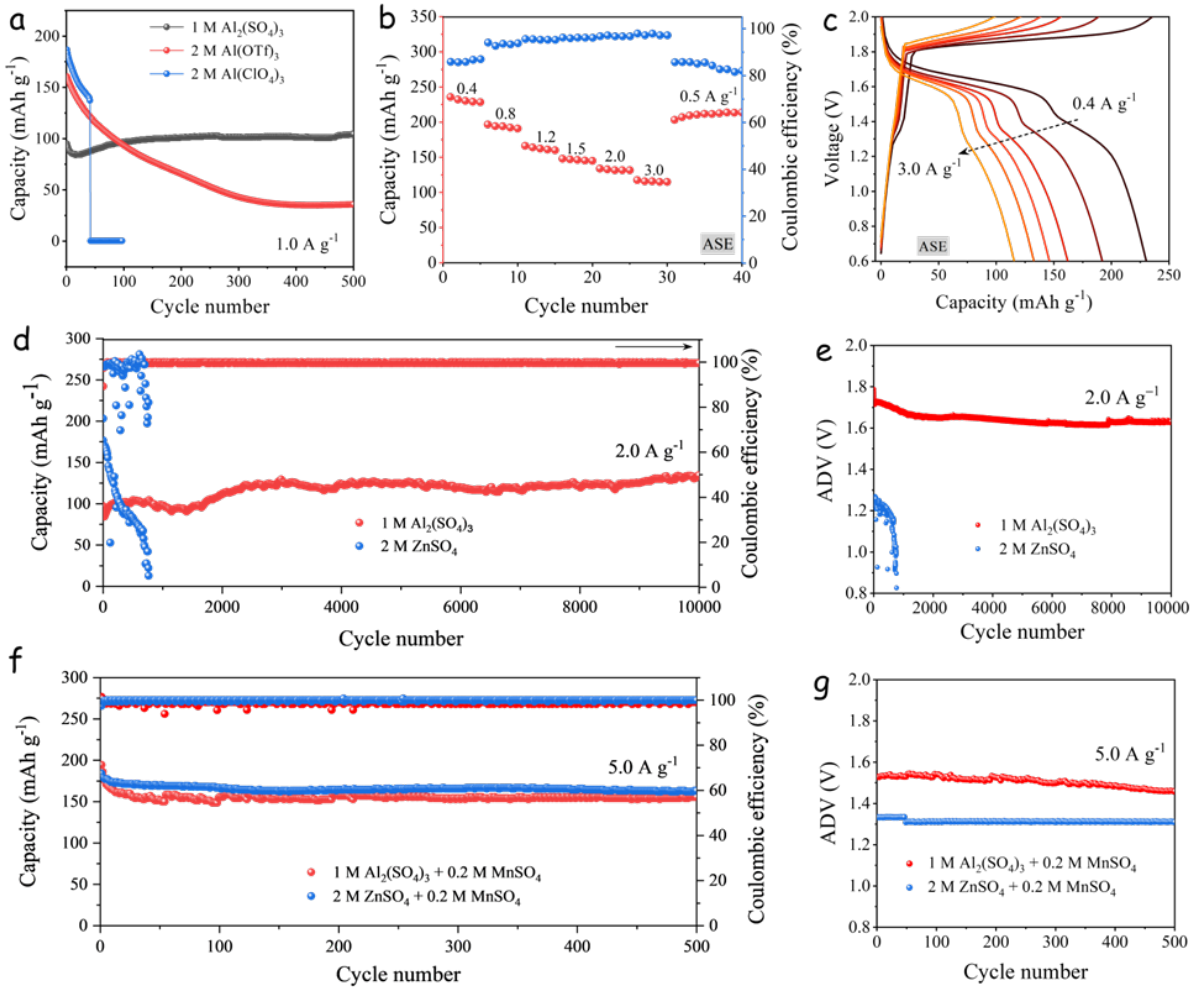

Figure 3. Electrochemistry of Zn-MnO_2 coin cells with Al^{3+} electrolytes. (a) Comparison of the cycle performance of Zn-MnO_2 batteries at 1 $A \cdot g^{-1}$ with the different Al-based electrolytes. (b) Rate performance of the ASE Zn-MnO_2 battery and (c) galvanostatic charge-discharge at different current densities. (d) Cycling performance and (e) ADV test at 2 $A \cdot g^{-1}$. (f) Cycling performance and (g) ADV test with 0.2 M $MnSO_4$ as an additive at 2 $A \cdot g^{-1}$.

Despite the relatively high capacity of conventional Zn-MnO_2 batteries based on ZSE, the fast decay makes them impractical. Moreover, the conventional Zn-MnO_2 battery has an initial energy efficiency of close to 80% that rapidly decreases (Figure S3c). In contrast, the Zn-MnO_2 battery based on ASE shows stable energy conversion efficiency above 80%. Besides, the ADV of the ASE Zn-MnO_2 cell stays above 1.6 V for 10,000 cycles denoting a highly reversible Al^{3+}-related capacitance mechanism (Figure 3e). In contrast, the conventional Zn-MnO_2 battery

tested here shows a significantly lower and much less stable ADV (~1.3 V), which is consistent with previously reported values.[15,23,24,25]

Additional cells were assembled incorporating $ZnSO_4$ within the ASE electrolyte but the obtained performance was inferior to that of the ASE-based batteries, as observed in Figure S4, probably due to a competing effect between the two ions. Reducing the $Al_2(SO_4)_3$ concentration to incorporate $ZnSO_4$ results in a stronger zinc intercalation discharge plateau and weaker discharge plateau at 1.6 V, indicating that the high discharge plateau is related to the ASE concentration.

To improve the electrochemical performance of conventional ZSE-based Zn-MnO_2 batteries, $MnSO_4$ is frequently used as an electrolyte additive to maximize the Mn^{2+} electrolysis process, promote accessibility of the electrode/electrolyte interface, and prevent excessive dissolution of MnO_2, which results in enhanced capacity and stability.[14, 24] As shown in Figure 3g, the cycle performance of both types of Zn-MnO_2 cells, the ASE- and the ZSE-based, is improved with the addition of 0.2 M $MnSO_4$. Both cells display similar capacity when cycled at 5 $A \cdot g^{-1}$. However, the ASE Zn-MnO_2 battery maintains a higher ADV than the ZSE Zn-MnO_2 (Figure 3f), i.e. a higher energy density.

As shown in Figures 4a and 4c, at 0.3 $A \cdot g^{-1}$, the ASE-based cell without $MnSO_4$ displays a high specific capacity of 469 $mAh \cdot g^{-1}$ and an ADV of 1.75 V, corresponding to an energy density of approximately 750 $Wh \cdot kg^{-1}$, based on the mass of MnO_2. Meanwhile, the ASE battery with 0.2 M $MnSO_4$ as additive exhibits lower capacity fading, a specific capacity >440 $mAh \cdot g^{-1}$ and an ADV of 1.66 V vs. Zn^{2+}/Zn, corresponding to an energy density of ~720 $Wh \cdot kg^{-1}$. These energy densities are comparable to those of high energy density Li-ion batteries, Li *vs.* NCM811 ($LiNi_{0.8}Co_{0.1}Mn_{0.1}O_2$), ~750 $Wh \cdot kg^{-1}$ with a 2.7–4.3 V voltage window at 0.1 C (1C= 200 $mAh \cdot g^{-1}$), based on the cathode mass. [26]

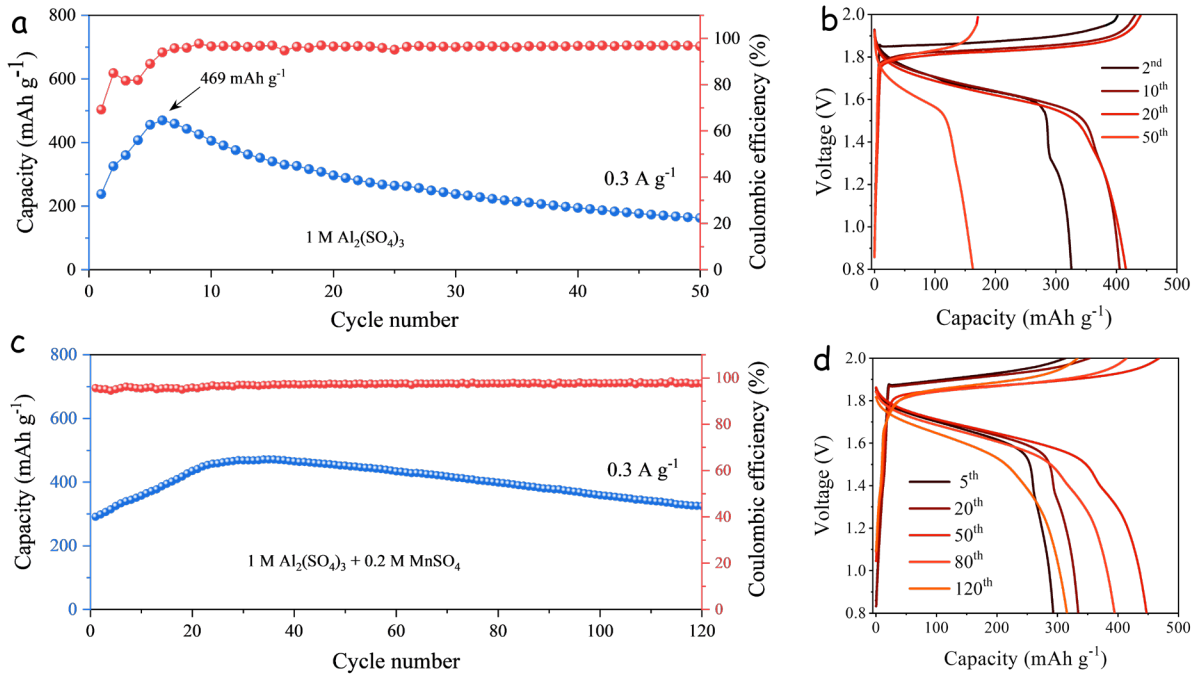

Figure 4. Cycling performance of new Zn-MnO_2 battery at 0.3 $A \cdot g^{-1}$. (a) Cycling performance and (b) galvanostatic charge-discharge profiles without $MnSO_4$ additive. (c) Cycling performance and (d) galvanostatic charge-discharge profiles with 0.2M $MnSO_4$ additive.

The ASE was characterized by a lower pH than the ZSE. To separate the effect of pH from that of the $Al_2(SO_4)_3$, we compared the performance of cells having different $Al_2(SO_4)_3$ concentrations but similar pH, adjusted with the addition of a small amount of H_2SO_4. Figure S5 shows the initial galvanostatic charge-discharge curves at 0.3 $A \cdot g^{-1}$ of three batteries based on an ASE, containing 0.4 M $Al_2(SO_4)_3$ + 0.02 M H_2SO_4 (pH= 3.3); 0.4 M $Al_2(SO_4)_3$ (pH= 4.1); and 0.8 M $Al_2(SO_4)_3$ (pH= 3.1). The addition of 0.02 M H_2SO_4 to the 0.4 M $Al_2(SO_4)_3$ electrolyte significantly improves the capacity, from about 110 mAh g^{-1} to about 280 mAh g^{-1}. However, adding a larger amount of $Al_2(SO_4)_3$ to reach a similar pH value resulted in a much larger capacity increase, above 400 mAh g^{-1}, thus demonstrating the important role played by Al^{3+} in the battery capacity.

To elucidate the mechanism resulting in the observed ADV increase in δ-MnO_2/CNT cathodes with the ASE, the structural evolution of δ-MnO_2/CNT was *ex situ* characterized during the discharge process. All electrodes were analyzed by XRD after 5 cycles at different discharge voltages (Figure 5a). Upon cycling, *ex situ* XRD patterns show new diffraction peaks assigned to $AlMn_2O_4$ and $ZnMn_2O_4$, at 1.5 V and 1.2 V (Zn^{2+}/Zn, discharge process), respectively. The characteristic XRD peak at 30.5° and 30.8° are attributed to $AlMn_2O_4$ (*Fd3m* of space group);

and 26.6° and 36.3° are the characteristic peaks of $ZnMn_2O_4$. The $ZnMn_2O_4$ and $AlMn_2O_4$ fingerprints were observed at 1.2 V and 1.5 V in the discharge process, respectively. To eliminate the effect of the carbon cloth, the active material powder was removed from the full-discharged electrode and further analyzed by XRD (Figures S6 and S7). The characteristic peaks of MnOOH (26º and 34º), Mn_3O_4 (32°, 36°and 44º) and MnO (20º, 22º and 27°) were observed.

Meanwhile, the Mn valence state was tested XANES for fully discharged and fully discharged electrodes. As shown in Figure 5b, the absorption edge peak of the fully discharged electrode split into two peaks (shown by the dotted line in the figure) and the energy of the edge absorption curves follows the order MnO < electrode < Mn_2O_3 < MnO_2, which proves that Mn^{2+} and Mn^{3+} substances present in the electrode. For the fully charged electrode (Figure 5c), the edge absorption fits the Mn^{4+} chemical state.[27-31] Overall, *ex situ* XRD and XANES analyses demonstrated the presence of Mn^{2+} and Mn^{3+} within different states in the fully discharged electrode, thus pointing to a capacitance contributed by several different mechanisms.

According to previous reports,[6, 32] in acidic electrolytes, the Mn^{4+}/Mn^{2+} redox reaction can contribute to the capacitance with a relatively high discharge plateau, >1.5 V, while the Mn^{4+}/Mn^{3+} associated with Zn^{2+} and H^+ intercalation contributes with a discharge plateau at a lower potential, ~1.2-1.5 V vs. Zn^{2+}/Zn. [6, 32] Thus, taking into account previous works, our electrochemical characterization results, and the *ex situ* XRD data, we propose the multi-ion cathodic reaction mechanism of the ASE-based Zn-MnO_2 battery to be as follows (excluding the intermediate Mn^{3+} reaction):

$$3MnO_2 + 2Al^{3+} + 6e^- \leftrightarrow AlMn_2O_4 + MnO \quad (2)$$

$$MnO_2 + 2H^+ + 2e^- \leftrightarrow MnO + 2H_2O \quad (3)$$

$$MnO + 2MnO_2 + 4H^+ + 2e^- \leftrightarrow Mn_3O_4 + H_2O \quad (4)$$

$$MnO_2 + H^+ + e^- \leftrightarrow MnOOH \quad (5)$$

$$Zn^{2+} + 2MnO_2 + 2e^- \leftrightarrow Zn\text{-}MnO_2 \quad (6)$$

Two Mn^{4+}/Mn^{2+} mechanisms associated with the reaction of Al^{3+} and H^+ with the MnO_2 to form $AlMn_2O_4$ and MnO, respectively (reactions (2) and (3)), contribute to the high discharge plateau >1.5 V vs. Zn^{2+}/Zn (Fig. 5d). [33] Besides, H^+ intercalation in MnO_2 as shown in reactions (4) and (5) contributes to an intermediate voltage discharge plateau, at ~1.4 V vs. Zn^{2+}/Zn. Finally, Zn^{2+} intercalation and de-intercalation in the MnO_2 crystal structure, reaction (6), contributes to the low voltage ~1.3 V vs. Zn^{2+}/Zn plateau.

To further confirm this assignment, the evolution of the CV curves and charge-discharge profiles with the cycle number and the current rate were analyzed. Figure S8 displays the 50 first CV curves of a fresh coin cell cycled at a sweep rate of 0.5 $mV \cdot s^{-1}$. The discharge peak around ~1.3 V gradually strengthens while the peak at 1.6 V becomes weaker. This evolution is consistent with the contribution of Al^{3+} ions to the capacity to gradually decrease, while the Zn^{2+} contribution increases as the number of cycles proceeds.

Due to the Lewis strong acid and strong electrostatic repulsion of multivalent ions such as Al^{3+}, the relative contribution of H^+ increases with the current rate. At low current, e.g. 0.3 $A \cdot g^{-1}$, the Al^{3+} intercalation has a significant contribution, which accelerates the capacity degradation owing to its large size (Figure 4a).[34-37] At high current rates, the H^+ contribution strongly dominates, Zn^{2+} and Al^{3+} ions have a marginal contribution due to their slower kinetics, and thus the stability is highly enhanced. Figure S9 shows the characteristic peak from dQ/dV corresponding to the Zn^{2+} intercalation at 0.3 $A \cdot g^{-1}$. However, the Mn^{4+}/Mn^{2+} oxidation peak is only observed at 2 $A \cdot g^{-1}$, implying that the high discharge plateau is related to the H^+ contribution. On the other hand, despite its relatively large size and coulombic repulsion, the discharge platform associated with the Zn^{2+} intercalation gradually increases with the charge-discharge cycling, up to 2.0 $A \cdot g^{-1}$ (Figure S10). Besides, as the cell cycles, MnO_2 inevitably dissolves in acidic conditions, thus Mn^{2+} ions accumulate in the solution and play a similar role as the $MnSO_4$ additive, increasing the cell capacity, as shown in Figure 3f. [33,38-40]

Taking into account the above experimental results, we hypothesize Al^{3+} ions play a role not only by intercalating into the MnO_2 to form $AlMn_2O_4$ but also by contributing to the Mn^{4+}/Mn^{2+} high voltage solid state conversion (reaction (3)).[33, 41] This contribution is associated with the release of protons during the Al^{3+} desolvation process, thus H^+ and Al^{3+} intercalaction into the MnO_2 during the cell discharge takes place, which is supported by the observation of the Al_2MnO_4 formation. Besides, we observe the solvated Al^{3+} to protect the Zn anode from corrosion in strong acidic electrolytes, preventing HER, which also contributes to the cell stability.

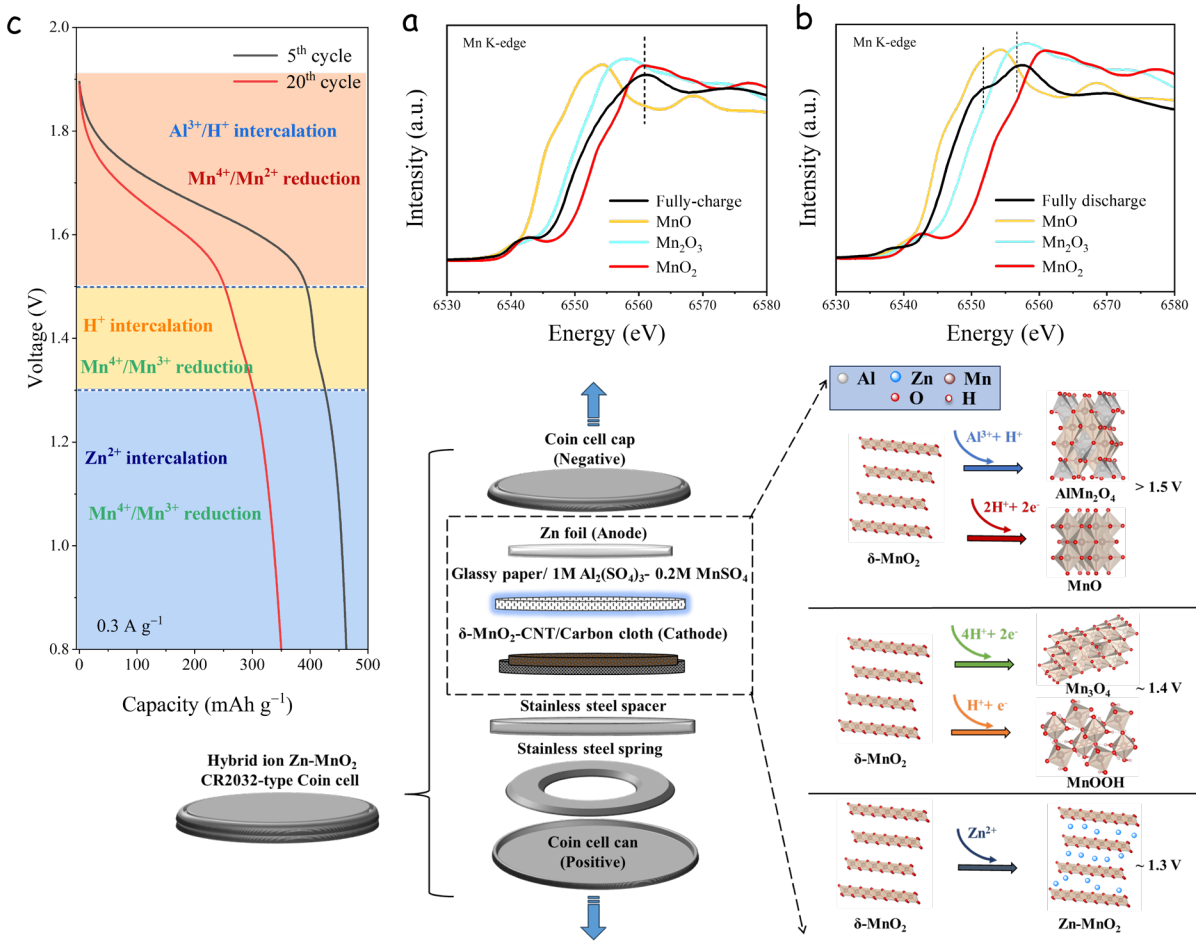

Figure 5. Mn K-edge XANES spectrum of (a) the fully discharged electrode and (b) the fully charged electrode. (c) Schematics of multi-ions reaction mechanism in the ASE Zn-MnO battery during the discharge process.

We further assembled ASE-based Zn-MnO_2 batteries with a high cathode mass loading to verify their potential for industrialization.[42] Figures 6a and 6b depict the galvanostatic charge-discharge curves at a current density of 2 A·cm^{-2} of a conventional ZSE Zn-MnO_2 battery with a mass loading of 6.4 mg·cm^{-2} and an ASE Zn-MnO_2 battery with 6.2 mg·cm^{-2} mass loading. In both batteries, we included 0.2 M $MnSO_4$ as an additive to promote the Mn^{4+}/Mn^{2+} contribution. Even at this high cathode loading, the two cells maintain significant capacity and cyclability. The galvanostatic charge-discharge curves show different voltage plateaus in both discharge and charge processes. In the conventional ZSE Zn-MnO_2 battery, the voltage plateaus correspond well to the two-step H^+/Zn^{2+} insertion/extraction processes. On the ASE Zn-MnO_2 battery, only one voltage plateau in the charge and discharge process at ~1.65 V is observed in the first few cycles associated with the two Mn^{4+}/Mn^{2+} processes. As the cycle progresses, an additional small discharge plateau at around 1.40 V, corresponding to H^+ insertion in MnO_2, is

obtained. Even at this high mass loading, the ASE battery still exhibits a higher AVD (1.55 V) than the conventional ZSE Zn-MnO_2 battery (1.35 V) related to the more significant weight within the ASE battery of the reversible Mn^{4+}/Mn^{2+} reaction within the measured capacity (Figure 6c). While similar capacities were obtained for both batteries (Fig. 6d), owing to the higher AVD, the ASE Zn-MnO_2 battery has a significantly higher energy density than the conventional ZSE Zn-MnO_2.

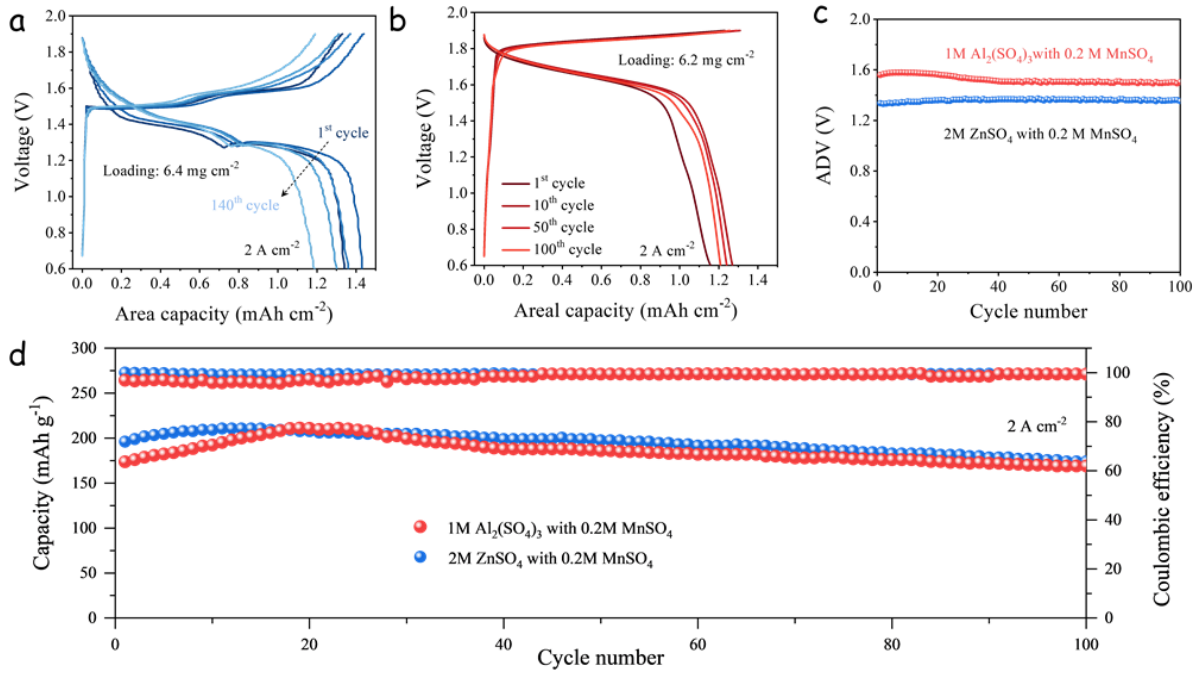

Figure 6. High mass-loading cells at 2 A·cm^{-2}. (a,b) Galvanostatic charge-discharge at different cycles of a conventional ZSE Zn-MnO_2 cell (a) and a new hybrid ASE Zn-MnO_2 cell (b). (c) ADV test. (d) Cycling performance.

3. Conclusions

An Al^{3+}-enabled high–voltage and stable Zn-MnO_2 battery displaying improved voltage, capacity, and energy density was demonstrated. Compared to the previously reported Zn-MnO_2 batteries based on a $ZnSO_4$ electrolyte, the MnO_2 cathode within an Al–ion electrolyte exhibits a highly reversible Mn^{4+}/Mn^{2+} reaction contributing to a high voltage discharge plateau (>1.5 vs. Zn^{2+}/Zn). The Al-based Zn-MnO_2 full cell delivered an ADV of ~1.75 V, a specific capacity of >450 mAh·g^{-1}, and energy densities up to 750 Wh·kg^{-1} at 0.3 A·g^{-1}, comparable to those of conventional Li-ion batteries. While in the conventional Zn-MnO_2 battery with 2M $ZnSO_4$ electrolyte, the performance decays very fast (less than 500 cycles with two discharge plateaus at ~1.4 V and 1.3 V), the new Zn-MnO_2 battery with 1 M $Al_2(SO_4)_3$ electrolyte shows a stable

capacity for over 10,000 cycles at 2.0 $A \cdot g^{-1}$. Even at 6.2 $mg \cdot cm^{-2}$ cathode mass-loading, a high ADV is obtained. Combining electrochemical analysis with *ex situ* XRD characterization, different mechanisms associated with Al^{3+}, H^{+}, and Zn^{2+} insertion/de–insertion and reaction were proposed to contribute to the battery capacitance. The outstanding performance of the Zn-MnO_2 battery based on the Al^{3+} was associated with both the highly reversible Al^{3+} ions intercalation/de-intercalation that significantly contributes to capacitance at low current rates and its positive effect on the Mn^{4+}/Mn^{2+} solid state reaction aided by H^{+} that dominates the capacitance at higher current rates. The performance of the ASE-based Zn-MnO_2 battery is expected to be further improved through rational design and engineering of the electrolyte and electrode parameters, such as an optimized pH, $Al_2(SO_4)_3$ concentration, incorporation of additives, or electrode coating/doping.

Acknowledgments

J. Chacón-Borrero and X. Chang contributed equally to this work. This work was supported by the project SyDECat (PID2022-136883OB-C22), financed by the Spanish MCIN/AEI, EHAWEDRY (964524), financed by European EXCELLENT SCIENCE – Further and Emerging Technologies, the National Natural Science Foundation of China (52272054, 52125105, 52061160484, 51972329), Natural Science Foundation of Guangdong Province (2019TX05L389, 2022A1515011365, 2024A1515011670), Shenzhen Science and Technology Planning Project (GJHZ20220913142809019, JCYJ20200109115624923), the Foundation of the National Research Council of Thailand (N42A650253), and the NSRF via the Program Management Unit for Human Resources & Institutional Development, Research and Innovation (B50G670108). Thanks to the China Scholarship Council (CSC) for the scholarship support. Part of the present work has been performed in the framework of Universitat Autònoma de Barcelona Materials Science PhD program.

Reference

1. Zhang Q, Dou Y, He Q, Deng S, Huang Q, Huang S, et al. Emerging Carbonyl Polymers as Sustainable Electrode Materials for Lithium-Free Metal-Ion Batteries. Energy Environ Mater. 2022;5(4):1037–59.

2. Li R, Li M, Chao Y, Guo J, Xu G, Li B, et al. Hexaoxacyclooctadecane induced interfacial engineering to achieve dendrite-free Zn ion batteries. Energy Storage Mater [Internet]. 2022;46(September 2021):605–12. Available from: https://doi.org/10.1016/j.ensm.2021.11.015

3. Guo Q, Li W, Li X, Zhang J, Sabaghi D, Zhang J, et al. Proton-selective coating enables fast-kinetics high-mass-loading cathodes for sustainable zinc batteries. Nat Commun.

2024;15(1).

4. Li G, Sun L, Zhang S, Zhang C, Jin H, Davey K, et al. Developing Cathode Materials for Aqueous Zinc Ion Batteries: Challenges and Practical Prospects. Adv Funct Mater. 2024;34(5).

5. Cui S, Zhang D, Gan Y. Traditional Electrochemical Zn2+ Intercalation/Extraction Mechanism Revisited: Unveiling Ion-Exchange Mediated Irreversible Zn2+ Intercalation for the δ-MnO2 Cathode in Aqueous Zn Ion Batteries. Adv Energy Mater. 2024;14(7):1–11.

6. Chao D, Zhou W, Ye C, Zhang Q, Chen Y, Gu L, et al. An Electrolytic Zn–MnO 2 Battery for High-Voltage and Scalable Energy Storage . Angew Chemie. 2019;131(23):7905–10.

7. Liu C, Chi X, Yang C, Liu Y. High-Voltage Aqueous Zinc Batteries Achieved by Trifunctional Metallic Bipolar Electrodes. Energy Environ Mater. 2023;6(1):1–8.

8. Huang J, Wang Z, Hou M, Dong X, Liu Y, Wang Y, et al. Polyaniline-intercalated manganese dioxide nanolayers as a high-performance cathode material for an aqueous zinc-ion battery. Nat Commun [Internet]. 2018;9(1):1–8. Available from: http://dx.doi.org/10.1038/s41467-018-04949-4

9. Zhang N, Cheng F, Liu J, Wang L, Long X, Liu X, et al. Rechargeable aqueous zinc-manganese dioxide batteries with high energy and power densities. Nat Commun [Internet]. 2017;8(1):1–9. Available from: http://dx.doi.org/10.1038/s41467-017-00467-x

10. Zhang N, Cheng F, Liu Y, Zhao Q, Lei K, Chen C, et al. Cation-Deficient Spinel ZnMn2O4 Cathode in Zn(CF3SO3)2 Electrolyte for Rechargeable Aqueous Zn-Ion Battery. J Am Chem Soc. 2016;138(39):12894–901.

11. Song M, Tan H, Chao D, Fan HJ. Recent Advances in Zn-Ion Batteries. Adv Funct Mater. 2018;28(41):1–27.

12. Zhang N, Ji YR, Wang JC, Wang PF, Zhu YR, Yi TF. Understanding of the charge storage mechanism of MnO2-based aqueous zinc-ion batteries: Reaction processes and regulation strategies. J Energy Chem [Internet]. 2023;82:423–63. Available from: https://doi.org/10.1016/j.jechem.2023.03.052

13. Wang H, Wang T, Stevenson G, Chamoun M, Lindström RW. MnO2/Mn2+ chemistry: Charging protocol and electrolyte regulation. Energy Storage Mater. 2023;63(October).

14. Cui S, Zhang D, Gan Y. The effect of Mn2+ additives on the capacity of aqueous Zn/δ-MnO2 batteries: Elucidating the Mn2+ concentration dependence of the irreversible transformation of δ-MnO2. J Power Sources. 2023;579(May).

15. Lv H, Song Y, Qin Z, Zhang M, Yang D, Pan Q, et al. Disproportionation enabling reversible MnO2/Mn2+ transformation in a mild aqueous Zn-MnO2 hybrid battery. Chem Eng J. 2022;430(September 2021).

16. Wang D, Liu Z, Gao XW, Gu Q, Zhao L, Luo W Bin. Massive anionic fluorine substitution two-dimensional δ-MnO2 nanosheets for high-performance aqueous zinc-ion battery. J Energy Storage [Internet]. 2023;72(PE):108740. Available from: https://doi.org/10.1016/j.est.2023.108740

17. Lee S, Jin W, Kim SH, Joo SH, Nam G, Oh P, et al. Oxygen Vacancy Diffusion and Condensation in Lithium-Ion Battery Cathode Materials. Angew Chemie - Int Ed. 2019;58(31):10478–85.

18. Gao P, Metz P, Hey T, Gong Y, Liu D, Edwards DD, et al. The critical role of point defects

in improving the specific capacitance of Î-MnO 2 nanosheets. Nat Commun. 2017;8.

19. Hu W, Ju J, Deng N, Liu M, Liu W, Zhang Y, et al. Recent progress in tackling Zn anode challenges for Zn ion batteries. J Mater Chem A. 2021;9(46):25750–72.

20. Gopalakrishnan M, Ganesan S, Nguyen MT, Yonezawa T, Praserthdam S, Pornprasertsuk R, et al. Critical roles of metal–organic frameworks in improving the Zn anode in aqueous zinc-ion batteries. Chem Eng J [Internet]. 2023;457(October 2022):141334. Available from: https://doi.org/10.1016/j.cej.2023.141334

21. Nie W, Cheng H, Sun Q, Liang S, Lu X, Lu B, et al. Design Strategies toward High-Performance Zn Metal Anode. Small Methods. 2023;2201572:1–28.

22. Lamprecht X, Speck F, Marzak P, Cherevko S, Bandarenka AS. Electrolyte Effects on the Stabilization of Prussian Blue Analogue Electrodes in Aqueous Sodium-Ion Batteries. ACS Appl Mater Interfaces. 2022 Jan 19;14(2):3515–25.

23. Xiaoyu Liu, Jin Yi, Kai Wu, Yong Jiang, Yuyu Liu, Bing Zhao, Wenrong Li JZ. Rechargeable Zn-MnO2 batteries: advances, challenges and perspectives. Nanotechnology [Internet]. 2020;31 (12):1–49. Available from: https://iopscience.iop.org/article/10.1088/2053-1583/abe778

24. Sun W, Wang F, Hou S, Yang C, Fan X, Ma Z, et al. Zn/MnO2 Battery Chemistry with H+ and Zn2+ Coinsertion. J Am Chem Soc. 2017;139(29):9775–8.

25. Aguilar I, Lemaire P, Ayouni N, Bendadesse E, Morozov A V., Sel O, et al. Identifying interfacial mechanisms limitations within aqueous Zn-MnO2 batteries and means to cure them with additives. Energy Storage Mater. 2022;53(June 2022):238–53.

26. Maleki Kheimeh Sari H, Li X. Controllable Cathode–Electrolyte Interface of Li[Ni0.8Co0.1Mn0.1]O2 for Lithium Ion Batteries: A Review. Adv Energy Mater. 2019;9(39):1–31.

27. Wu D, Housel LM, King ST, Mansley ZR, Sadique N, Zhu Y, et al. Simultaneous Elucidation of Solid and Solution Manganese Environments via Multiphase Operando Extended X-ray Absorption Fine Structure Spectroscopy in Aqueous Zn/MnO2Batteries. J Am Chem Soc. 2022;144(51):23405–20.

28. Farges F. Ab initio and experimental pre-edge investigations of the Mn K -edge XANES in oxide-type materials. Phys Rev B - Condens Matter Mater Phys. 2005;71(15):1–14.

29. Jiang Y, Yuan L, Wang X, Zhang W, Liu J, Wu X, et al. Jahn–Teller Disproportionation Induced Exfoliation of Unit-Cell Scale ϵ-MnO 2 . Angew Chemie. 2020;132(50):22848–55.

30. Yao S, Wang S, Liu R, Liu X, Fu Z, Wang D, et al. Delocalizing the d-electrons spin states of Mn site in MnO2 for anion-intercalation energy storage. Nano Energy [Internet]. 2022;99(May):107391. Available from: https://doi.org/10.1016/j.nanoen.2022.107391

31. Yadav PL, Shelke AR, Wang HT, Chen KH, Lin WX, Li CW, et al. Mn3+ eg Configuration and Electron Transfer in Na-Incorporating α-MnO2 to Improve Electrochemical Supercapacitor: An In Situ and Ex Situ X-ray Absorption Spectroscopic Investigation. ACS Appl Energy Mater. 2023;6(12):6443–55.

32. Qin Z, Song Y, Yang D, Zhang MY, Shi HY, Li C, et al. Enabling Reversible MnO2/Mn2+Transformation by Al3+Addition for Aqueous Zn-MnO2Hybrid Batteries. ACS Appl Mater Interfaces. 2022 Mar 2;14(8):10526–34.

33. Li H, Firby CJ, Elezzabi AY. Rechargeable Aqueous Hybrid Zn2+/Al3+ Electrochromic Batteries. Joule [Internet]. 2019;3(9):2268–78. Available from: https://doi.org/10.1016/j.joule.2019.06.021

34. Xing L, Zhang C, Li M, Hu P, Zhang X, Dai Y, et al. Revealing excess Al3+ preinsertion on altering diffusion paths of aluminum vanadate for zinc-ion batteries. Energy Storage Mater [Internet]. 2022;52(May):291–8. Available from: https://doi.org/10.1016/j.ensm.2022.07.044

35. Gu S, Wang H, Wu C, Bai Y, Li H, Wu F. Confirming reversible Al3+ storage mechanism through intercalation of Al3+ into V2O5 nanowires in a rechargeable aluminum battery. Energy Storage Mater [Internet]. 2017;6:9–17. Available from: http://dx.doi.org/10.1016/j.ensm.2016.09.001

36. Lv H, Yang S, Li C, Han C, Tang Y, Li X, et al. Suppressing passivation layer of Al anode in aqueous electrolytes by complexation of H2PO4− to Al3+ and an electrochromic Al ion battery. Energy Storage Mater [Internet]. 2021;39(April):412–8. Available from: https://doi.org/10.1016/j.ensm.2021.04.044

37. Wu Z, Lian Z, Yan S, Li J, Xu J, Chen S, et al. Extraordinarily Stable Aqueous Electrochromic Battery Based on Li4Ti5O12and Hybrid Al3+/Zn2+Electrolyte. ACS Nano. 2022;16(8):13199–210.

38. Li N, Li G, Li C, Yang H, Qin G, Sun X, et al. Bi-Cation Electrolyte for a 1.7 V Aqueous Zn Ion Battery. ACS Appl Mater Interfaces. 2020;12(12):13790–6.

39. Li K, Gong Y, Lin JH. Benzoquinone-intercalated vanadium oxide in the electrolyte with Al3+ for zinc-ion storage: dual-pillar effect and reversible disorder–order conversion. Chem Eng J [Internet]. 2023;452(P4):139621. Available from: https://doi.org/10.1016/j.cej.2022.139621

40. Dou Q, Yao N, Pang WK, Park Y, Xiong P, Han X, et al. Unveiling solvation structure and desolvation dynamics of hybrid electrolytes for ultralong cyclability and facile kinetics of Zn-Al alloy anodes. Energy Environ Sci. 2022;15.

41. Balland V, Mateos M, Singh A, Harris KD, Laberty-Robert C, Limoges B. The Role of Al3+-Based Aqueous Electrolytes in the Charge Storage Mechanism of MnOx Cathodes. Small. 2021;17(23).

42. Kuang Y, Chen C, Kirsch D, Hu L. Thick Electrode Batteries: Principles, Opportunities, and Challenges. Adv Energy Mater. 2019;9(33):1–19.